EUROPEAN ORGANIZATION FOR NUCLEAR RESEARCH

CERN/EP 83-170
1 November 1983

INCLUSIVE π^0 PRODUCTION IN 360 GeV pp INTERACTIONS USING THE EUROPEAN HYBRID SPECTROMETER

EHS-RCBC Collaboration
Bombay[1]-CERN[2]-Genova[3]-Innsbruck[4]-Japan UG[5]-Madrid[6]-Mons[7]-Rutgers[8]-Serpukhov[9]-Tennessee[10]-Vienna[11] Collaboration

J.L. Bailly[7], W. Bartl[11], F. Bruyant[2], W.M. Bugg[10], C. Caso[2], R. Contri[3], H. Dibon[11], R. Di Marco[8], B. Epp[4], A. Ferrando[6], F. Fontanelli[3], P. Girtler[4], A. Gurtu[1], E.L. Hart[10], P. Herquet[7], J. Hrubec[2], Y. Iga[5(a)], E. Kistenev[9], S. Kitamura[5(a)], J.M. Kohli(*), H. Kohno[5(c)], J.C. Marin[2], M. Markytan[11], I.S. Mittra(*), L. Montanet[2], G. Neuhofer[11], Y. Petrovykh[9], R. Plano[8], B. Poljakov[9], P. Porth[11], B. Powell[2], T. Rodrigo[6], A.H. Rogers[10], J. Salicio[6], S. Squarcia[3], P. Stamer[8], V. Stopchenko[9], K. Sudhakar[1], U. Trevisan[3], C. Willmott[6], T. Yamagata[5(a)] and V. Yarba[9]

1 Tata Institute of Fundamental Research, Bombay, India
2 CERN, European Organization for Nuclear Research, Geneva, Switzerland
3 University of Genova and INFN, Italy
4 Inst. für Experimentalphysik, Innsbruck, Austria(+)
5(a) Tokyo Metropolitan University, Tokyo, Japan
(b) Tokyo University of Agriculture and Technology, Tokyo, Japan
(c) Chuo University, Tokyo, Japan
(d) Hiroshima University, Hiroshima, Japan
6 Junta de Energia Nuclear, Madrid, Spain
7 Université de l'Etat, Faculté des Sciences, Mons, Belgium
8 Rutgers University, New Brunswick, USA
9 I.H.E.P., Serpuhkov, USSR
10 University of Tennessee, Knoxville, USA
11 Inst. für Hochenergiephysik, Vienna, Austria(+)
(*) Punjab University, Chandigarh, India

Submitted to Zeitschrift für Physik C

(+) Supported by Fonds zur Förderung der Wissensch. Forschung.

1436P/CC/ed

ABSTRACT

The intermediate and forward gamma detectors of EHS are used to reconstruct π^o's produced by 360 GeV/c pp interactions in the Rapid Cycling Bubble Chamber (RCBC). The calibration of the gamma detectors is described. Using the pp forward-backward symmetry, the inclusive π^o production cross section is obtained $\sigma_{\pi^o} = (132 \pm 11)$mb. The average π^o multiplicity is determined as a function of the charged particle multiplicity. The (1-x) dependence is given for different p_T regions.

1. INTRODUCTION

In this work we report on π^o inclusive production in pp interactions at 360 GeV. The data of this experiment were obtained using the European Hybrid Spectrometer (EHS) associated with the hydrogen bubble chamber RCBC.

This paper is divided in two parts. First we describe briefly the EHS electromagnetic calorimeters, the calibration and monitoring procedures and the effects we had to correct for to obtain a good energy resolution (sects 2 and 3).

In the second part we discuss the $M(\gamma\gamma)$ spectra. The weighting procedure to take care of losses is explained in sect. 4. In sect. 5, using the backward-forward symmetry, we calculate the π^o cross section and the dependence of the average π^o multiplicity on the charged multiplicity.

In sect. 6 we discuss the π^o x and p_T distributions and the related structure functions.

2. THE PHOTON DETECTION SYSTEM

The complete set-up of EHS has been described elsewhere [1]; here we recall only the relevant aspects of the two electromagnetic calorimeters: the Intermediate Gamma Detector (IGD) and the Forward Gamma Detector (FGD).

The apparatus consists of two large arrays of lead glass blocks. The first one (IGD) is composed of 1122 blocks with a central hole matching the gap of the downstream magnet.

The second one (FGD) is made of 3 separate sections: a converter, a position detector, and an absorber for a total of 140 lead glasses and 375 scintillators.

To take into account the photomultiplier gain fluctuations a monitoring system based on a laser flash is used [2]. The light is distributed to all the counters via a system of optical fibers. The variation in the laser output is corrected by a high stability vacuum photodiode which allows to normalize the flash to the photodiode signal. In normal conditions the monitoring effect is not higher than a few per cent.

3. THE CALIBRATION PROCEDURE

Both calorimeters have been calibrated in a 40 GeV electron beam to obtain a set of calibration coefficients. A detailed description of the procedure is given in ref. [2].

The results described in this section are based upon the analysis of the calibration data collected before the data taking period.

The total number of recorded showers was 400,000. Before using the calibration data, several effects had to be estimated and corrected for. First of all the monitoring procedure was applied. The effect for one of the IGD counters is shown in fig. 1. Due to the high intensity of the electron beam there was a heating effect in the PM's which appeared as a drift of the gain during the spill. Because of the limited beam time available for the calibration, it was not possible to make the statistics large enough to estimate the rate dependence for the individual counters. Therefore, the variation of the PM gain as a function of the event number within the spill averaged over all the IGD counters has been used. Its value reaches ≃ 4.25% at the end of the spill.

The dependence of the light collection efficiency on the impact point coordinates is presented in fig. 2, where R is its distance from the centre of the counter. The maximum of the correction amounts to ≃ 3.4% in the corners of the lead glass blocks.

To avoid low energy electron contamination and the leakage downstream of the detector, only showers with energy above 35 GeV were finally accepted.

Fig. 3 shows the distribution of the shower energies as measured in IGD before (I) and after (II) corrections. The energy resolution (FWHM) amounts to 5.0% at 40 GeV.

Fig. 4 displays the energy distribution in FGD. The raw data were corrected for the rate dependence only (less than 1%).

To get an estimate of the position resolution in the IGD, the information from the upstream wire chambers were used to predict the impacts of charged tracks into the IGD front plane. The resolution for these predictions amounts to about 4 mm; taking into account a 5 mm resolution in the difference between the predicted and measured impact, our IGD position resolution turns out to be ≈ 3 mm.

4. WEIGHTING PROCEDURE

We shall discuss here some losses in π^o detection and the procedure used to correct them.

The real position of both detectors was slightly different from the designed one. In fact, the hole in IGD, the gap in the magnet and the FGD body did not fully match (this problem is widely treated in ref. [3]). As a consequence, some π^o's were not seen by the gamma detectors. In order to correct for these losses we have assigned to each observed event a weight inversely proportional to its detection probability.

To compute this weight, for each x and p_T interval, Monte-Carlo events were generated isotropically in the π^o centre of mass system and photons were traced down through the spectrometer.

We took into account the probability of γ interaction in the material in front of the calorimeters and we introduced a correction for overlapping showers. Since to reduce the hadronic background we discarded in the analysis all the showers with $E < 0.9$ GeV for IGD and $E < 2.$ GeV for FGD, the same cuts were also applied in the Monte-Carlo generation.

Finally, we considered the γ helicity angle in the π^o rest frame (θ^*). This distribution (not shown) is flat up to $\cos\theta^* \simeq 0.8$ but then it falls very steeply, so we cut there and corrected accordingly.

For IGD only, we tried to reject unwanted hadrons cutting on the lateral development of the showers. We checked that this procedure rejects at most 5% of the signal.

5. INCLUSIVE π^o CROSS SECTION

The data used in this analysis come from a sample of ~ 19000 interactions detected in the bubble chamber (1.8 μb/event). Details on scanning procedure and topological cross sections can be found in ref. [4].

The unweighted $M(\gamma\gamma)$ spectrum is shown in fig. 5 for γ-γ combinations belonging to IGD only (a), FGD only (b) and to both of them (mixed combinations only) (c). The sum of the corresponding weighted histograms is shown in fig. 6. The superimposed curve is the result of a fit with the function $y = A * M^B * \exp(-C * M - D * M^2)$ to reproduce the background, plus a gaussian to represent the signal.

The fit gives ~ 26400 π^o's; the central value and the width of the π^o peak are 0.1349 GeV and 0.0085 GeV respectively. To calculate the inclusive π^o cross section, we took into account the forward/backward symmetry of the p-p system; this gives $\sigma = (132 \pm 11)$mb. The quoted error includes both systematic and statistics: we estimate our statistical error of $\simeq$ 4%.

Fig. 7 shows the dependence of the π^o cross section on the incident proton laboratory momentum [6]. The solid curve represents a parametrization [7] of $(\sigma_{\pi^+} + \sigma_{\pi^-})/2$. The two dashed curves are the 10% estimated accuracy of the parametrization. Our data support the faster then logarithm law for the cross section growth suggested in ref. [6] for $P_{lab} > 100$ GeV/c. At our energy the above parametrization yields $\sigma_{\pi^+} = 125$ mb and $\sigma_{\pi^-} = 104$ mb. Taking into account a 10% accuracy on these values, we conclude that our point is compatible both with the central curve and with σ_{π^-} [6].

The π^o cross section and the average number of π^o's as a function of the total charged multiplicity n_{ch} are presented in figs 8(a) and 8(b) for different energies. A comparison is made with the known function $<\pi^o> = N_- + 0.4$ where N_- is the number of negative particles (mostly pions) in the event. In our experiment $<\pi^o>$ increases with increasing n_{ch}. This behaviour, also observed at 400 GeV/c [6], is different from the one found at 205 GeV/c [5] where $<\pi^o>$ is interpreted as increasing with n_{ch} only up to $n_{ch} \leq 14$, then decreasing. This reduction has been analyzed in some models (see, for example, ref. [8]) and seems to reflect limits imposed by the phase space. Of course, considering the large errors in our data at higher multiplicity,as well as our difficulty to derive reliable values of $<\pi^o>$ for $n_{ch} > 18$, we cannot exclude the possibility of a decreasing $<\pi^o>$ at high n_{ch}, but it is certain that, with respect to the 205 GeV/c data, the possible maximum in $<\pi^o>$ has moved toward higher values of n_{ch}. The linear dependence of $<\pi^o>$ on n_{ch} has been ascribed to some kind of cluster production mechanisms as required by the strong correlation of the isospin state of the pion. Excluding the 2-prong events, a linear fit was made giving a slope $a = .33 \pm .03$ which should be compared with the value $a \simeq .38$ predicted by the model in ref. [8]. It is worth noting that this slope (which is found to be negative for energies $\leq$ 15 GeV, as expected by considering the dominant part of the kinematics correlations) shows some saturation up to ISR energies, due to the increasing role played by the dynamics; furthermore, this slope turns out to be essentially independent of the nature of the incoming beam, indicating a sort of universality between the yields of neutral and charged particles. The average π^o multiplicity is 4.0 ± 0.4 in good agreement with the prediction from the relation $<\pi^o> = 1.51 \ln (0.512 \sqrt{s})$ fitted on ISR data [9]. The dependence of the KNO function $\psi(z) = (<n_{ch}>/<\pi^o>)(\sigma_n(\pi^o)/\sigma_{inel})$ (where $\sigma_n(\pi^o)$ is the π^o production cross section for a given charged multiplicity n) on $z = n_{ch}/<n_{ch}>$ is given in fig. 9. The solid curve is the result of a parametrization of p-p data from 69 to 305 GeV/c [10] with a polynomial function. Up to the charged multiplicity for which we can quote a π^o cross section ($n_{ch} \leq 20$), our data are consistent with a unified description of semi-inclusive π^o production cross sections.

In the part of the $M(\gamma\gamma)$ spectrum not included in fig. 6, no clear signal is visible for $\eta(550)$. For $|x| > 0.1$ its presence is revealed by a slightly enhanced shoulder. The cross section for η production can then be estimated to be ≃ 3.5 mb. For $|x| > 0.1$ we derive a η/π^o production ratio of ~ .22.

6. DIFFERENTIAL DISTRIBUTIONS

To determine π^o differential distributions we have used the usual procedure of fitting the $M(\gamma\gamma)$ spectrum as described above, for each bin of the relevant variable.

The differential cross section $d\sigma/dx$ and the relativistic invariant function $\frac{2E^*}{\pi\sqrt{s}}\frac{d\sigma}{dx}$ are displayed in figs 10(a) and 10(b). The latter is also shown for several p_T intervals in fig. 11. There the x invariant distributions have been fitted with the well known formula

$$\frac{2E^*}{\pi\sqrt{s}}\frac{d\sigma}{dx} = A\ (\ 1 - |x|)^{\alpha}$$

Results are given in table 1. For small p_T, the fits are rather poor.

In figs 12(a) and 12(b) we present the ds/dp_T^2 and the $\frac{2E^*}{\pi\sqrt{s}}\frac{d\sigma}{dp_T^2}$ distributions. The first distribution is well described by an expression $Ae^{-ap_T^2} + Be^{-bp_T^2}$, with $A = (695 \pm 36)(\text{mb/GeV}^2)$, $B = (69 \pm 13)(\text{mb/GeV}^2)$, $a = (7.9 \pm 0.5)\text{GeV}^{-2}$, $b = (2.3 \pm 0.2)\text{GeV}^{-2}$.

The π^o momentum distribution is shown in fig. 13. Its mean value is (17.6 ± 2.4)GeV indicating that almost 70 GeV are carried out by neutral pions. The average transverse momentum $<p_T>$ as a function of $|x|$ is plotted in fig. 14. The so-called "seagull effect" is clearly visible.

7. CONCLUSIONS

We have described in this paper the main features of the inclusive production of neutral pions in pp collisions at 360 GeV/c. The characteristics of the experimental apparatus for γ detection have also been discussed.

The total inclusive π^o cross section is found equal to (132 ± 11)mb. This value agrees with those reported at other energies and seems to support a non logarithmic dependence on p_{lab}. σ_{π^o} is compatible both with σ_{π^+} and σ_{π^-} at the same energy.

$<\pi^o>$ depends monotonically on the total charged multiplicity, the constant slope being .33 ± .03.

The average π^o multiplicity per inelastic event is 4.0 ± 0.4.

The η inclusive cross section turns out to be about 3.5 mb for $|x| > .1$, giving an η/π^o ratio of $\simeq .22$.

REFERENCES

[1] LEBC-EHS Collaboration, Nucl. Instr. and Meth. 205 (1983) 79.

[2] B. Powell et al., Nucl. Instr. and Meth. 198 (1982) 217.

[3] O. Tchikilev and G. Zumerle, π^0 reconstruction in EHS; CERN/EP/EHS/PH 82-5.

[4] Bombay-CERN-Genova-Innsbruck-Japan UG-Madrid-Mons-Rutgers-Serpukhov-Tennessee-Vienna Collaboration, Strange particle production in 360 GeV/c pp interactions using the European Hybrid Spectrometer, Submitted to the High Energy Physics Conference, Brighton (UK), 20-27 July 1983.

[5] K. Jaeger et al., Phys. Rev. D11 (1975) 2405.

[6] R.D. Kass et al., Phys. Rev. D20 (1979) 605.

[7] M. Antinucci et al., Lett. Nuovo Cim. 6 (1973) 121.

[8] G.H. Thomas, Phys. Rev. D8 (1973) 3042.

[9] G. Neuhofer et al., Phys. Lett. 38B (1972) 51 and 37B (1971) 438.

[10] F.T. Dao and J. Whitmore, Phys. Lett. B46 (1973) 252.

TABLE 1

Δp_T (GeV)	A	α
$0 < p_T < 0.15$	5.2 ± 0.4	26.1 ± 2.4
$0.15 < p_T < 0.3$	5.3 ± 0.5	9.6 ± 0.8
$0.3 < p_T < 0.5$	7.6 ± 0.6	8.9 ± 0.6
$0.5 < p_T < 1.0$	5.6 ± 0.4	6.6 ± 0.5

FIGURE CAPTIONS

Fig. 1 Distribution of the shower energy deposition measured in one of the counters before and after the monitoring procedure. Data before monitoring are arbitrarily imposed to peak at 40 GeV.

Fig. 2 Variation of the light collection efficiency as a function of the impact coordinates. The curve is to guide the eye.

Fig. 3 Distribution of the shower energy in IGD before (I) and after (II) all corrections.

Fig. 4 Energy distribution in FGD after all corrections.

Fig. 5 γ-γ effective mass for IGD (a), FGD (b), mixed (one γ in IGD, one in FGD) (c).

Fig. 6 γ-γ effective mass for both FGD and IGD with superimposed fit.

Fig. 7 π^o cross section as a function of p_{lab}. The solid curve is a parametrisation from ref. [7] (see also ref. [6] and refs therein).

Fig. 8 (a) π^o cross section as a function of the charged multiplicity.

(b) Average number of π^o's as a function of the charged multiplicity.

Fig. 9 KNO plot for π^o multiplicity distribution. The solid line is taken from ref. [10].

Fig. 10 $d\sigma/dx$ (a) and the invariant function $(2E^*/\pi\sqrt{s})d\sigma/dx$ (b) for π^o.

Fig. 11 The invariant distribution $(2E^*/\pi\sqrt{s})d\sigma/dx$ for several p_T intervals. See text for explanation of the fits.

Fig. 12 $d\sigma/dp_T^2$ (full points) (a) and the invariant function $(2E^*/\pi\sqrt{s})d\sigma/dp_T^2$ (open points) (b) for π^o. See text for explanation of the fit.

FIGURE CAPTIONS (Cont'd)

Fig. 13 π^o momentum distribution.

Fig. 14 π^o average transverse momentum $<p_T>$ as a function of x.

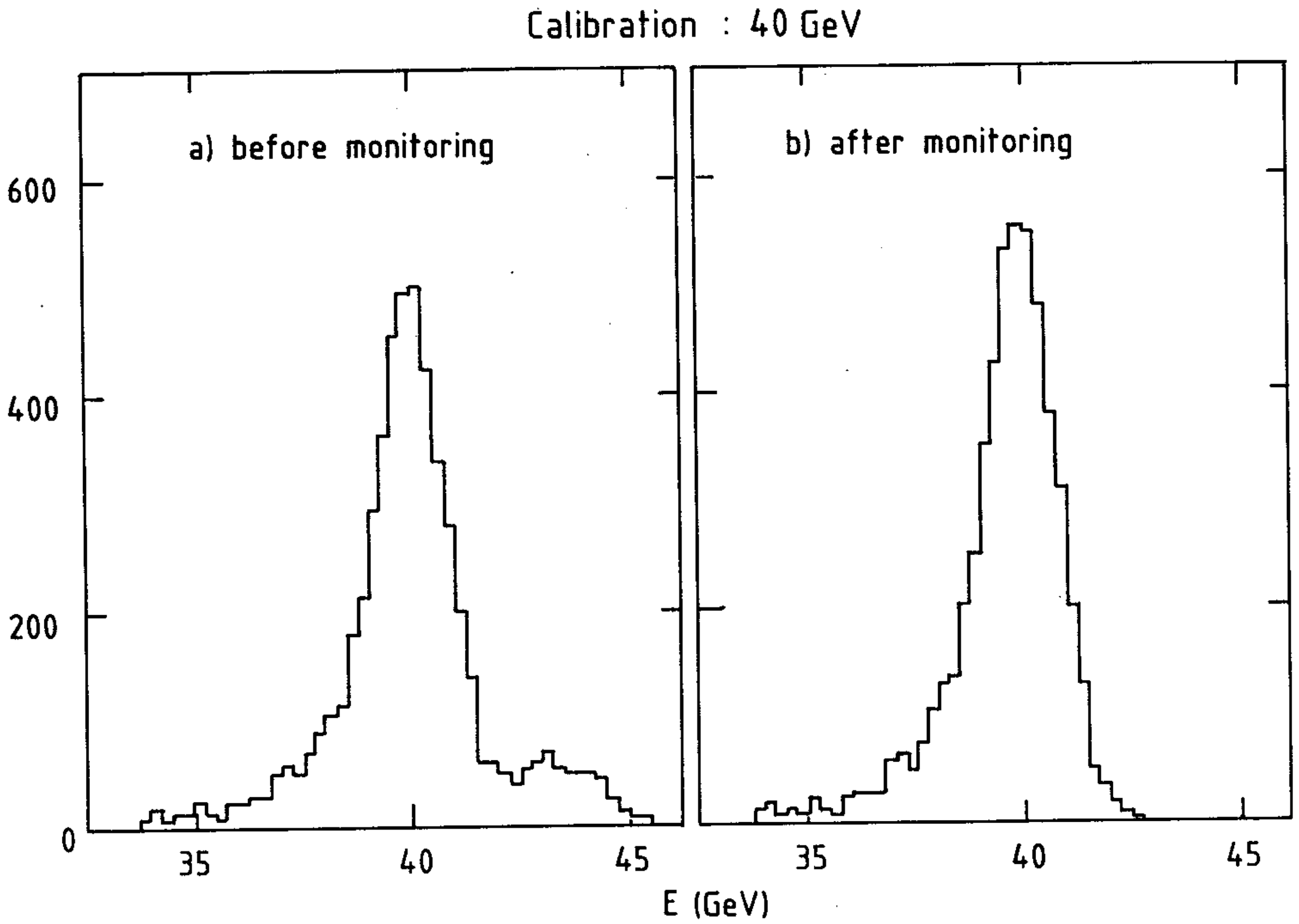
Calibration : 40 GeV
a) before monitoring
b) after monitoring
600
400
200
0
35
40
45
35
40
45
E (GeV)

Fig.1

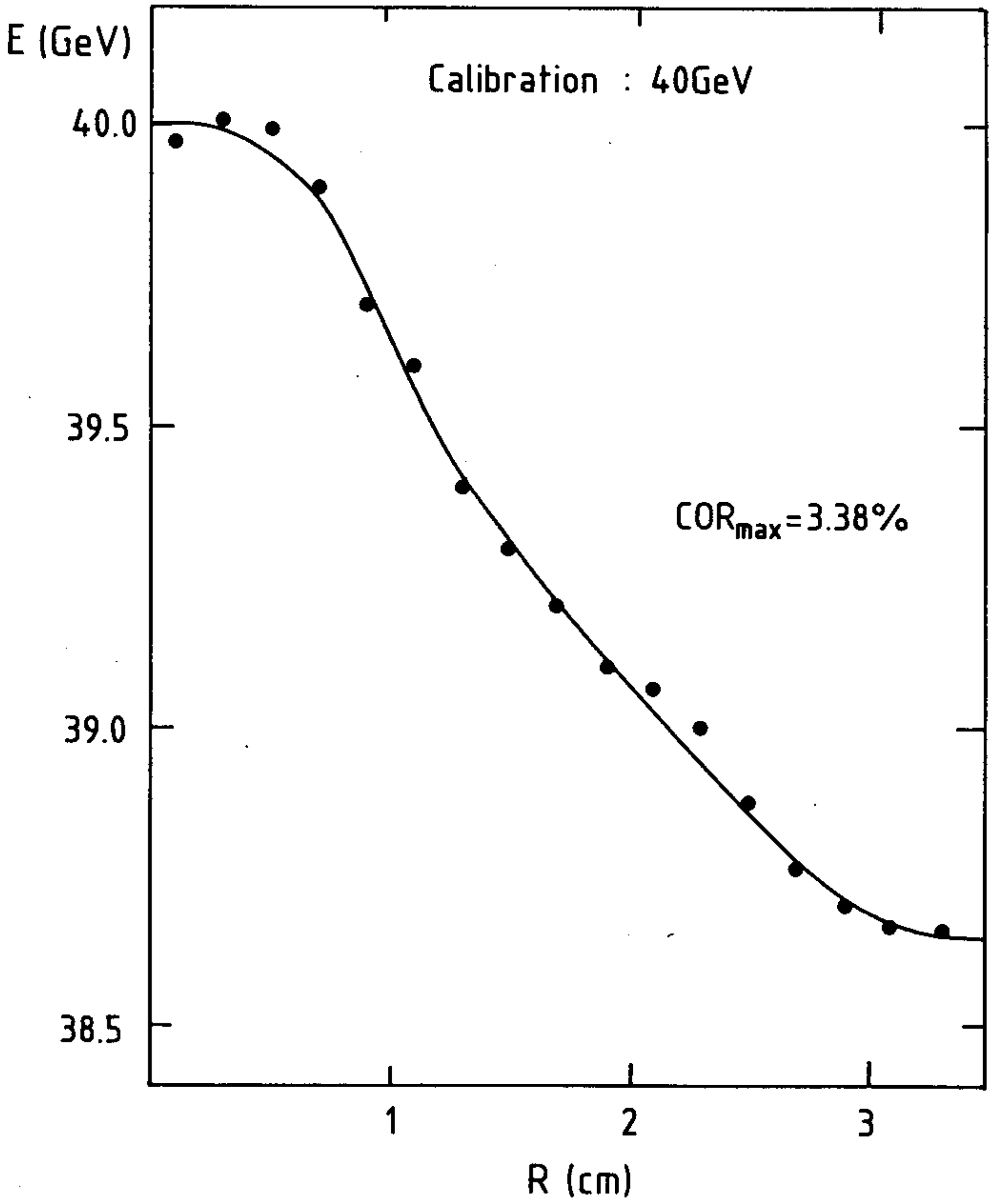

Fig.2

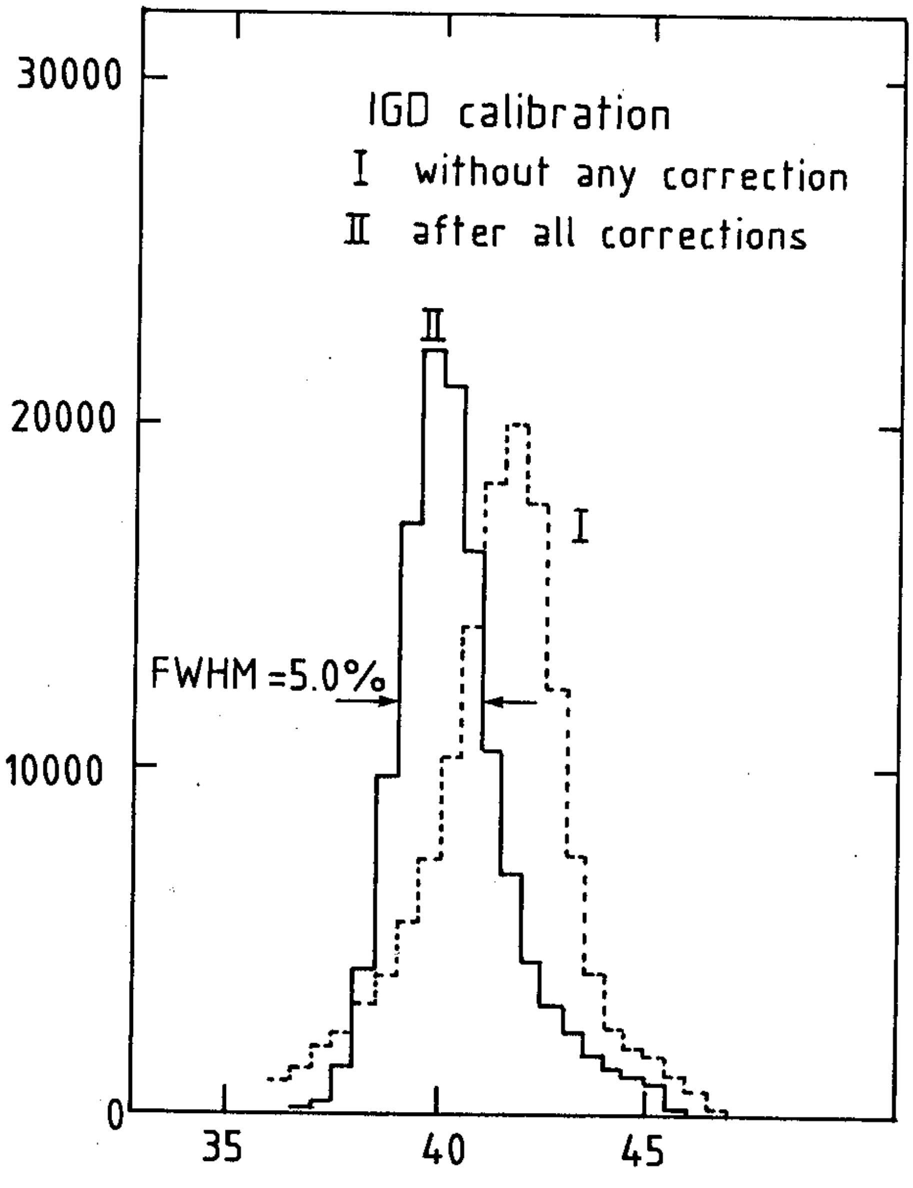

30000
20000
10000
0
35
40
45
E (GeV)
IGD calibration
I without any correction
II after all corrections
II
I
FWHM =5.0%

Fig.3

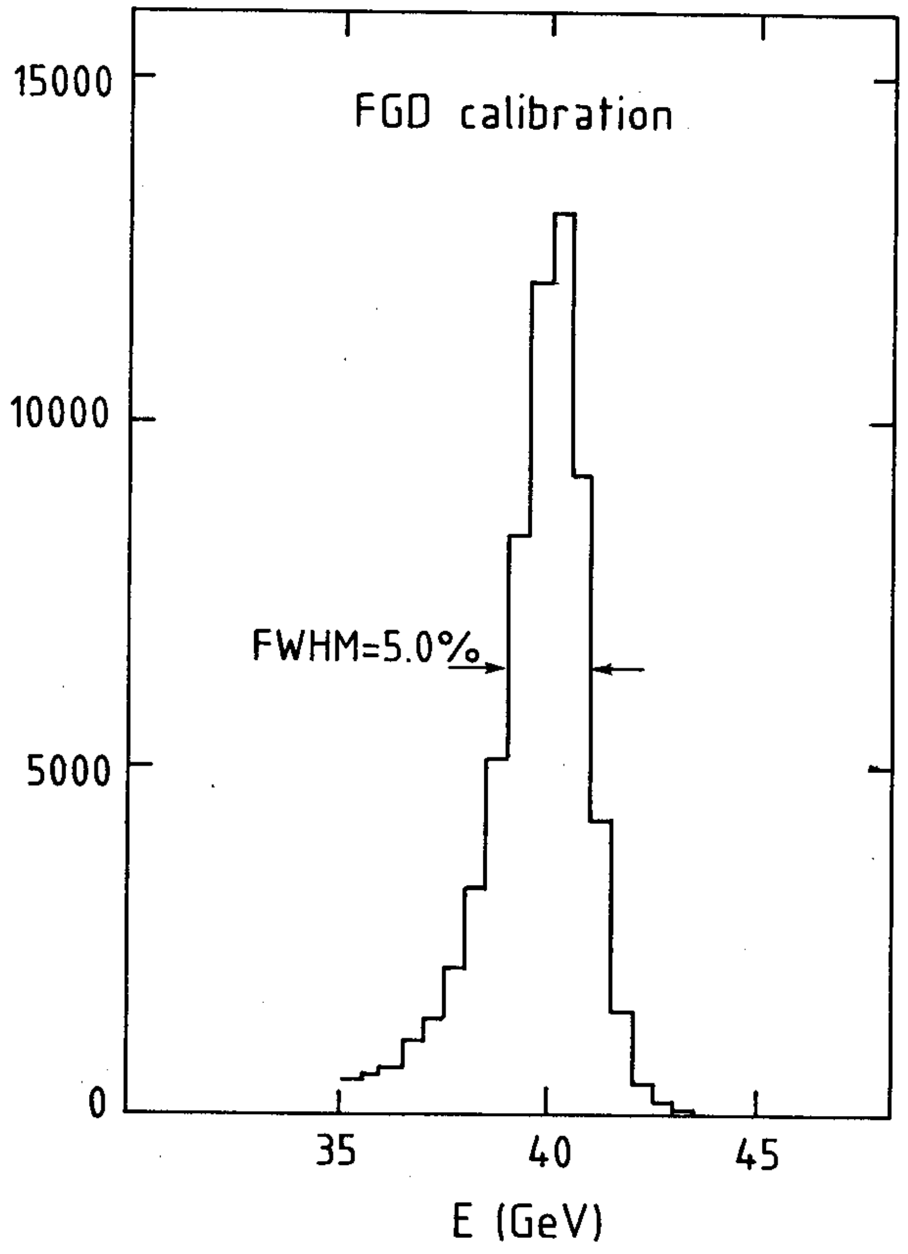

Fig.4

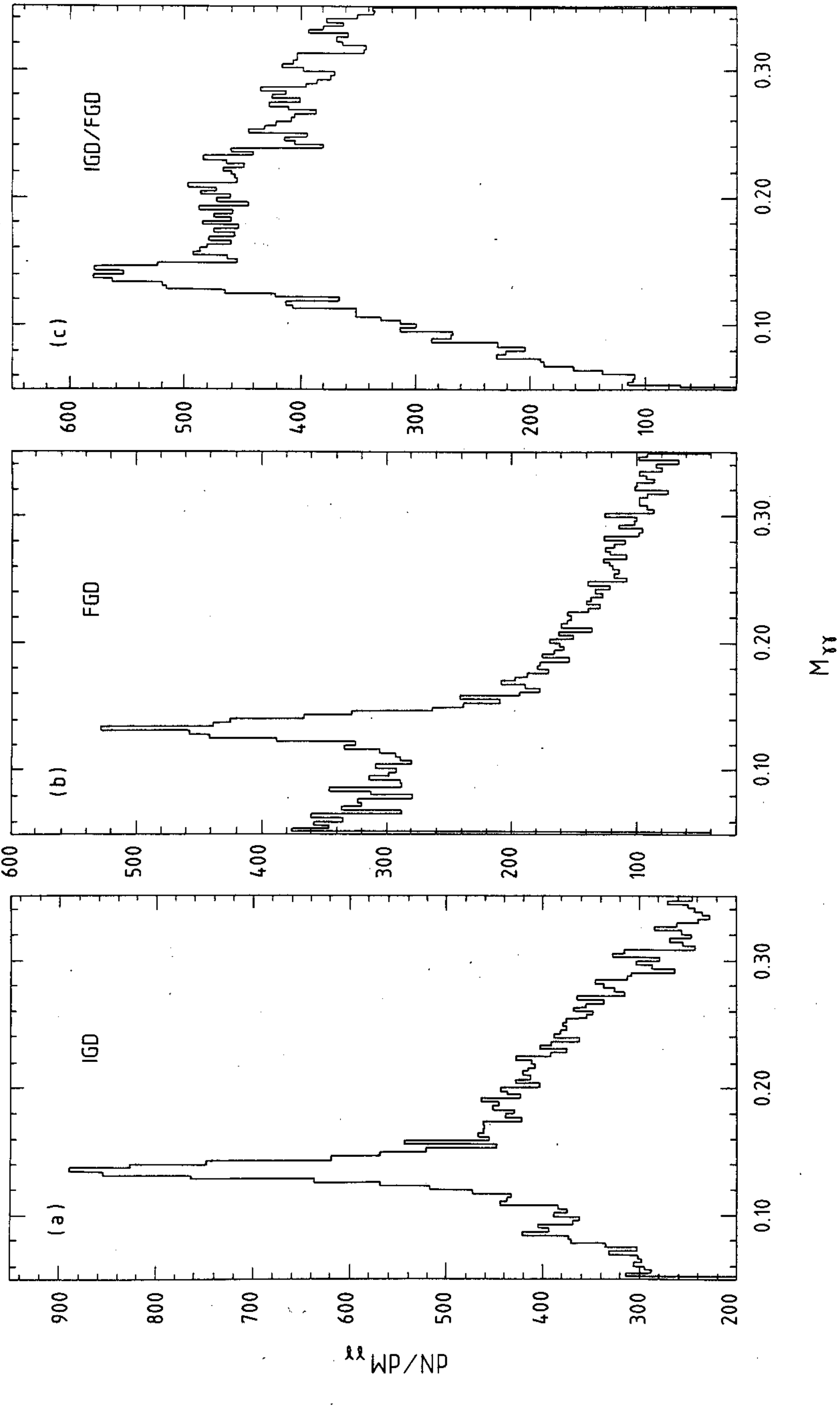
(a)
IGD
900
800
700
600
500
400
300
200
(b)
FGD
600
500
400
300
200
100
(c)
IGD/FGD
600
500
400
300
200
100
0.10
0.20
0.30
$M_{\gamma\gamma}$
$dN/dM_{\gamma\gamma}$

Fig.5

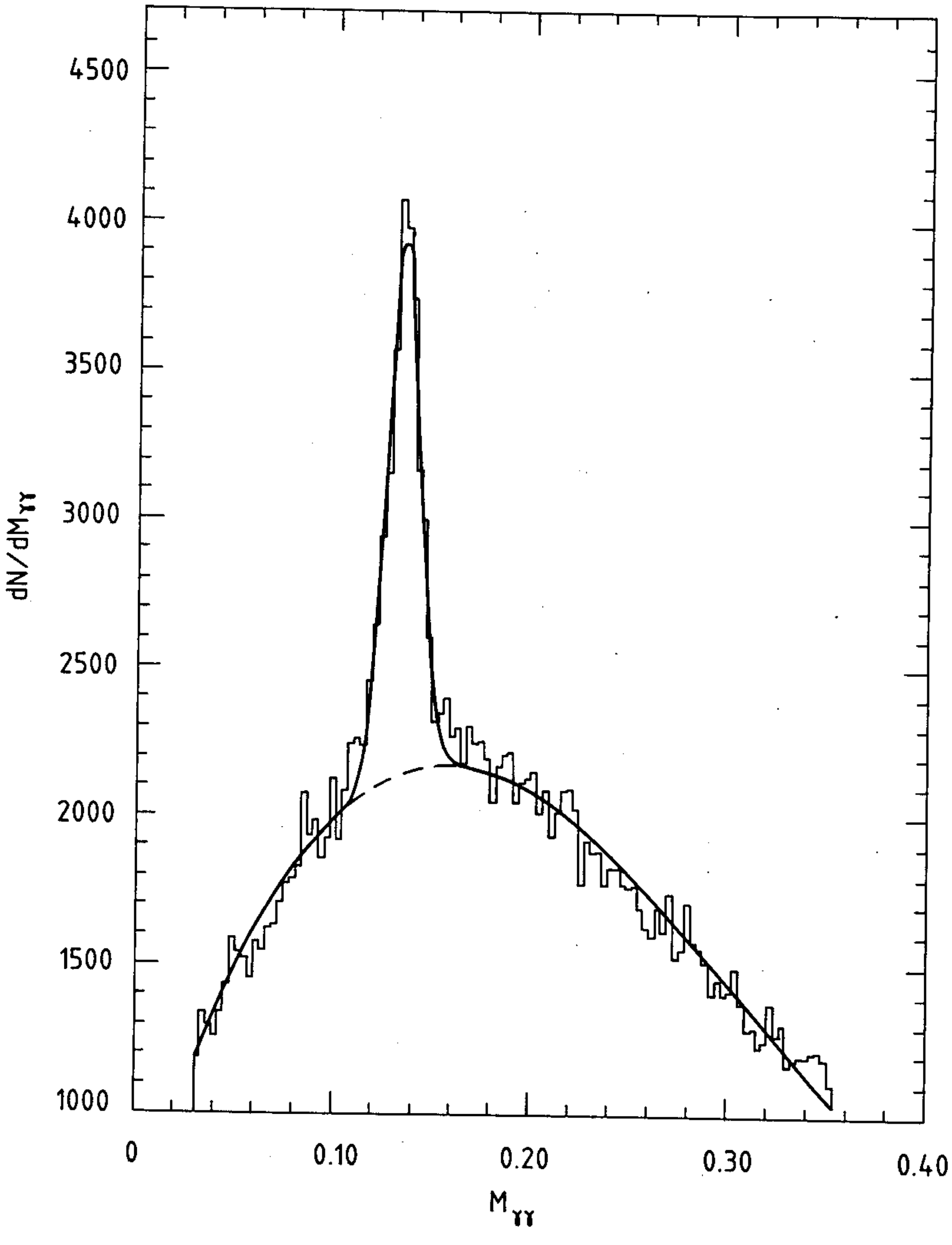
4500
4000
3500
3000
2500
2000
1500
1000
dN/dM$_{\gamma\gamma}$
0
0.10
0.20
0.30
0.40
M$_{\gamma\gamma}$

Fig.6

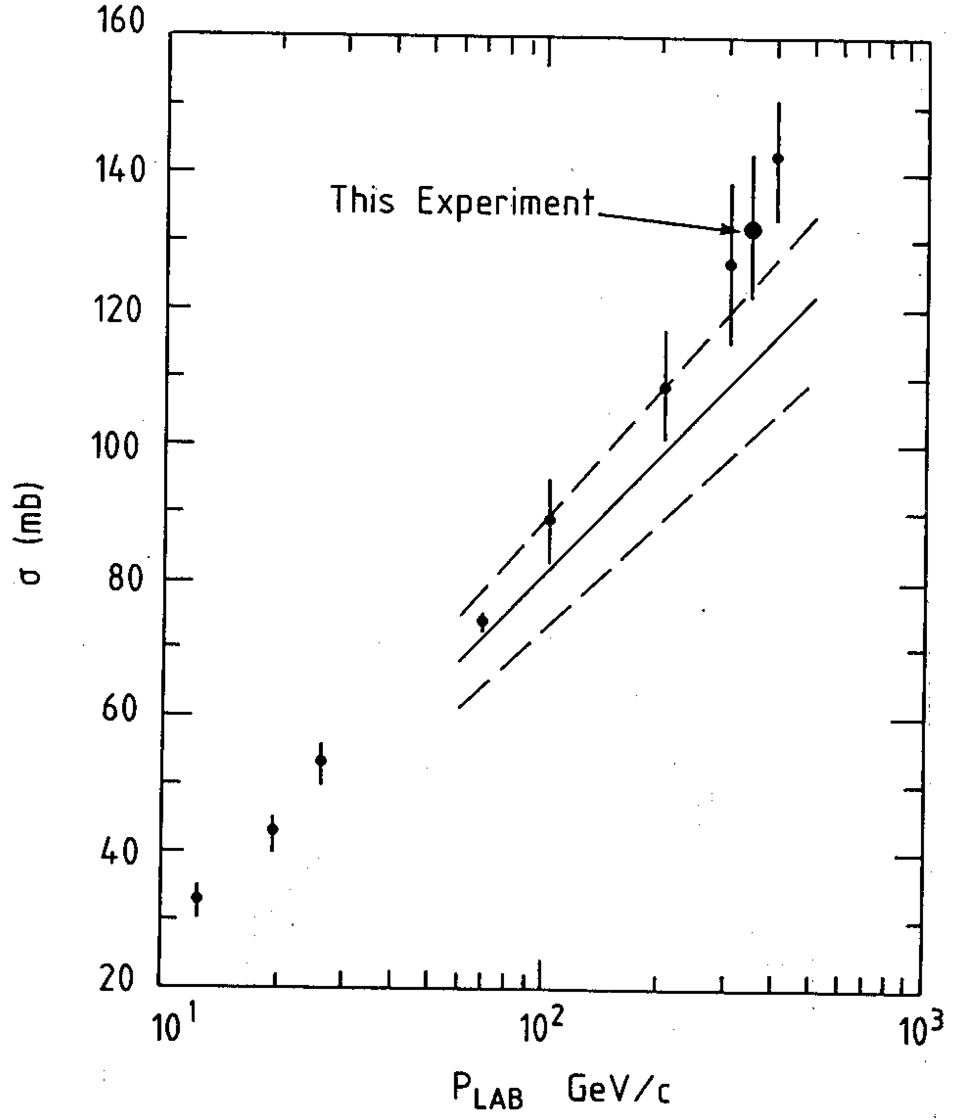
160
140
120
100
80
60
40
20
σ (mb)
This Experiment
10^1
10^2
10^3
P_{LAB} GeV/c

Fig. 7

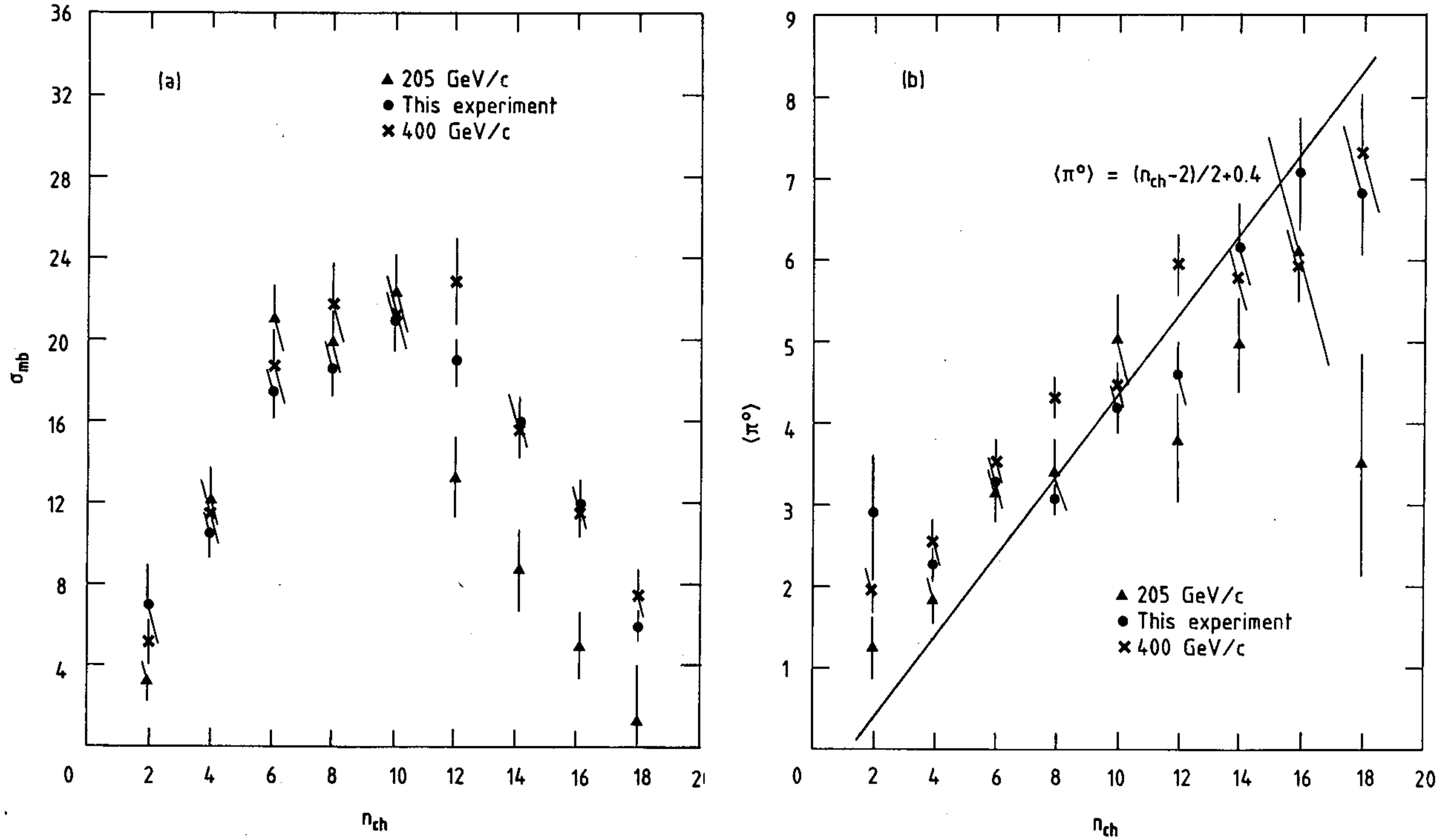
(a)
▲ 205 GeV/c
● This experiment
✖ 400 GeV/c
σ_{mb}
36
32
28
24
20
16
12
8
4
0
2
4
6
8
10
12
14
16
18
20
n_{ch}
(b)
$\langle\pi^o\rangle = (n_{ch}-2)/2+0.4$
▲ 205 GeV/c
● This experiment
✖ 400 GeV/c
$\langle\pi^o\rangle$
9
8
7
6
5
4
3
2
1
0
2
4
6
8
10
12
14
16
18
20
n_{ch}

Fig.8

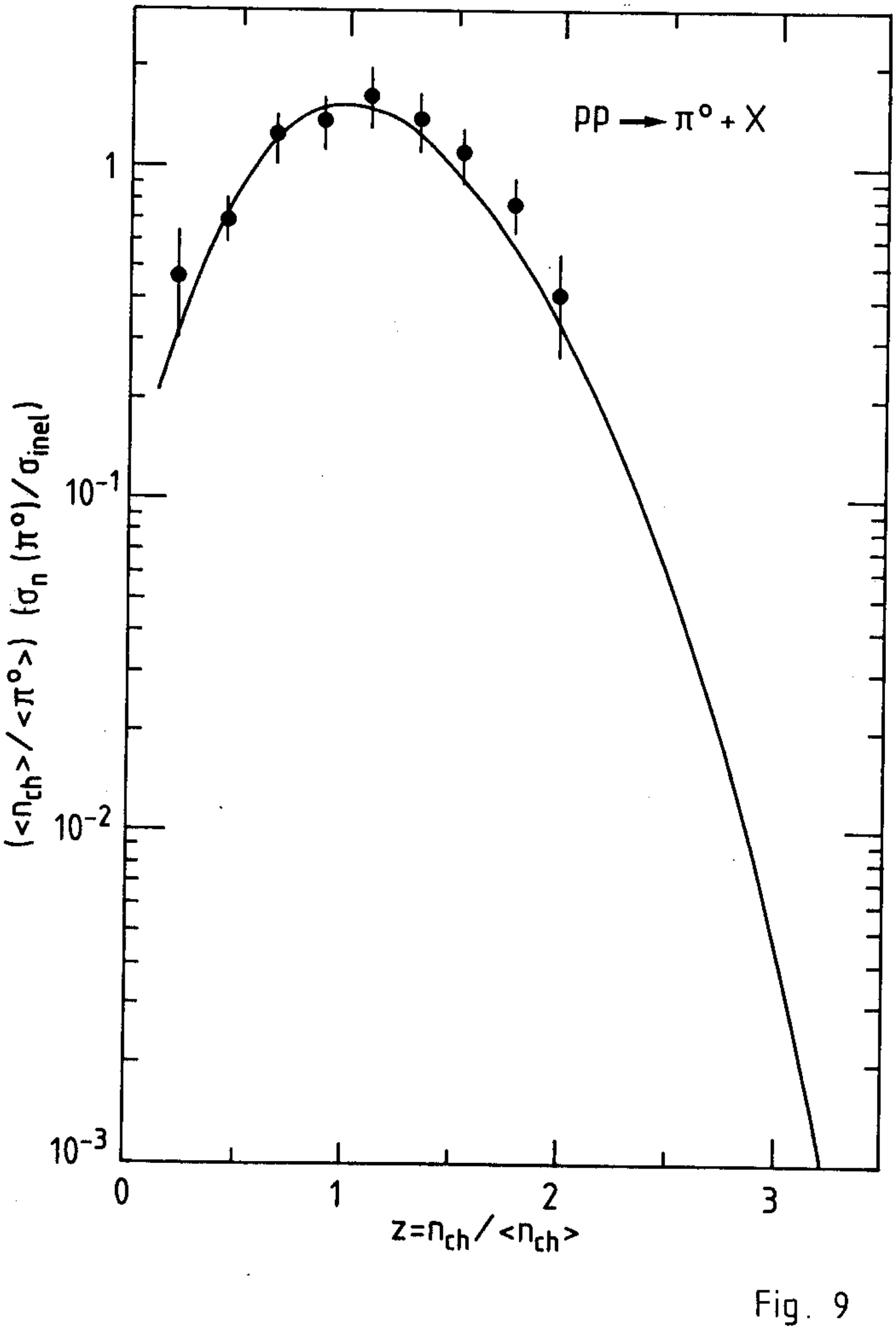

Fig. 9

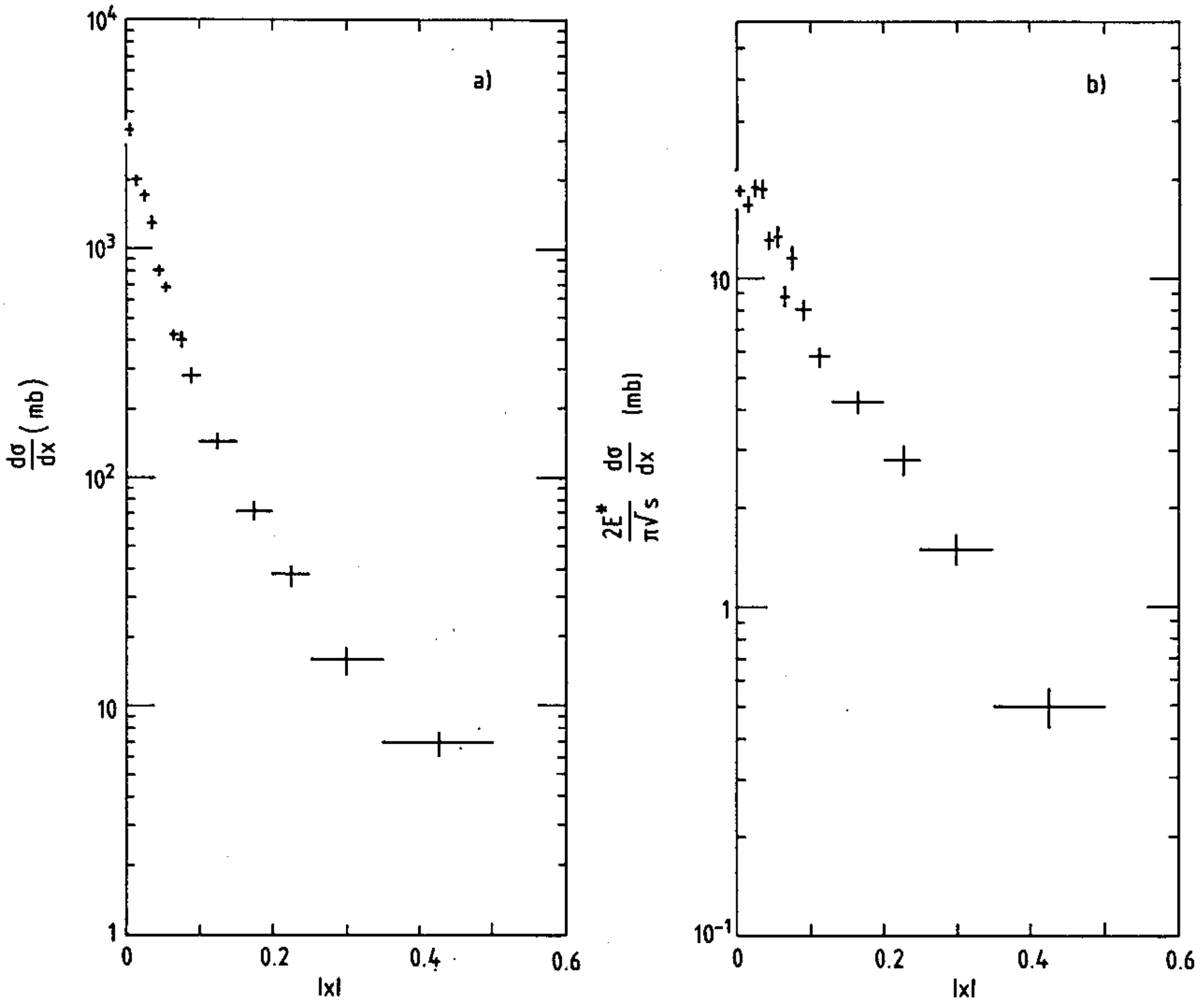
a)
10^4
10^3
10^2
10
1
$\frac{d\sigma}{dx}$ (mb)
0
0.2
0.4
0.6
|x|
b)
10
1
10^{-1}
$\frac{2E^*}{\pi\sqrt{s}} \frac{d\sigma}{dx}$ (mb)
0
0.2
0.4
0.6
|x|

Fig. 10

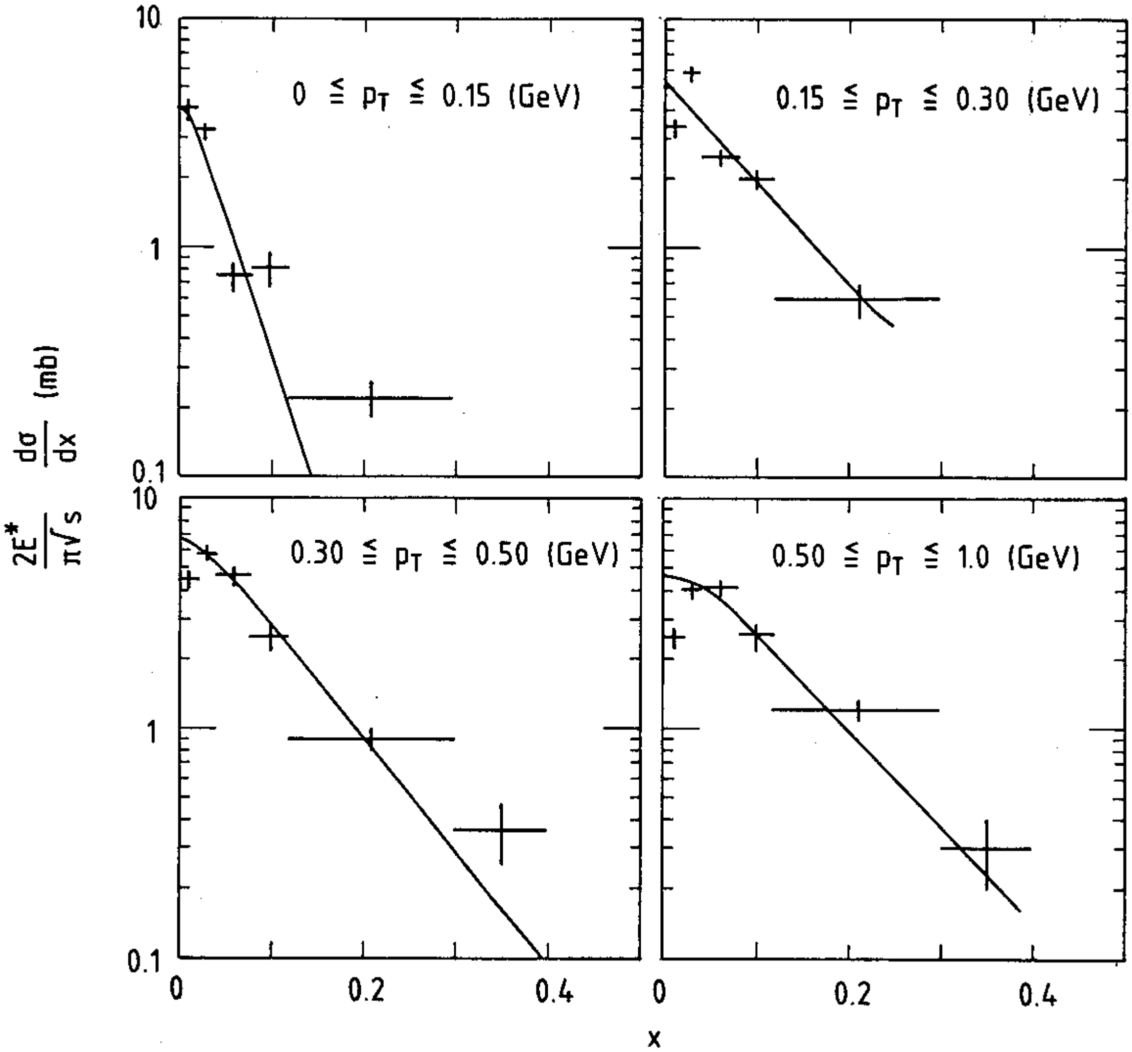
$0 \leqq p_T \leqq 0.15$ (GeV)
$0.15 \leqq p_T \leqq 0.30$ (GeV)
$0.30 \leqq p_T \leqq 0.50$ (GeV)
$0.50 \leqq p_T \leqq 1.0$ (GeV)
$\frac{2E^*}{\pi\sqrt{s}} \frac{d\sigma}{dx}$ (mb)
10
1
0.1
0
0.2
0.4
x

Fig. 11

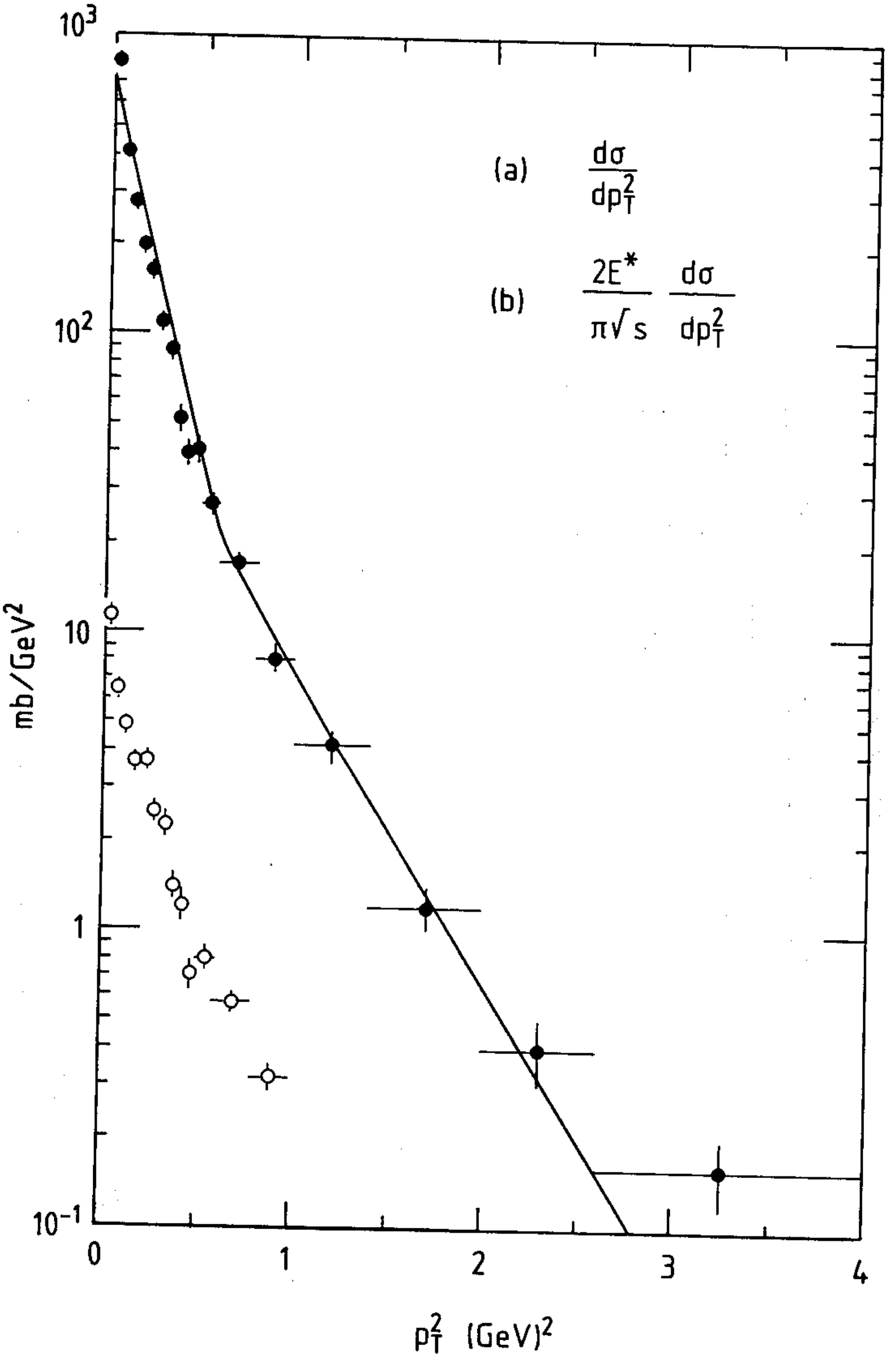

10^3
10^2
10
1
10^{-1}
mb/GeV^2
(a) $\frac{d\sigma}{dp_T^2}$
(b) $\frac{2E^*}{\pi\sqrt{s}} \frac{d\sigma}{dp_T^2}$
0
1
2
3
4
p_T^2 (GeV)^2

Fig. 12

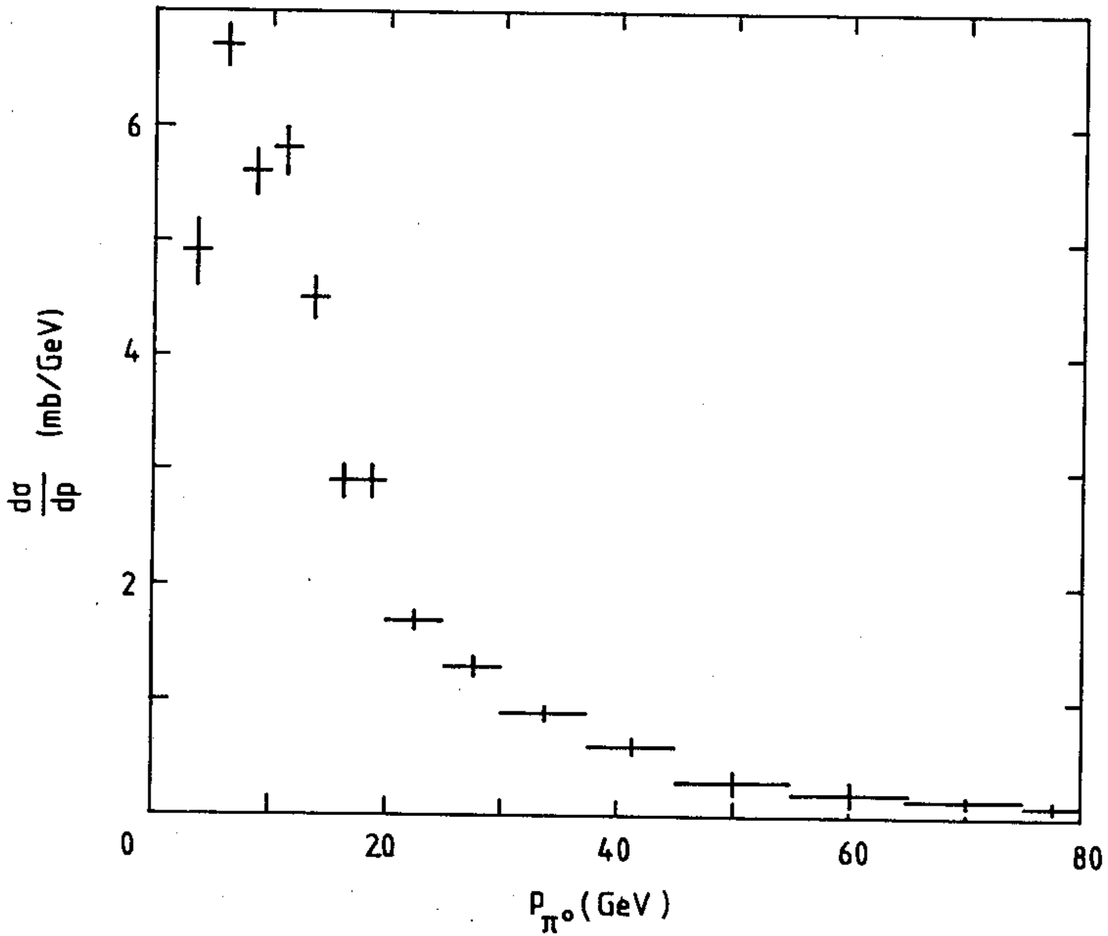

Fig. 13

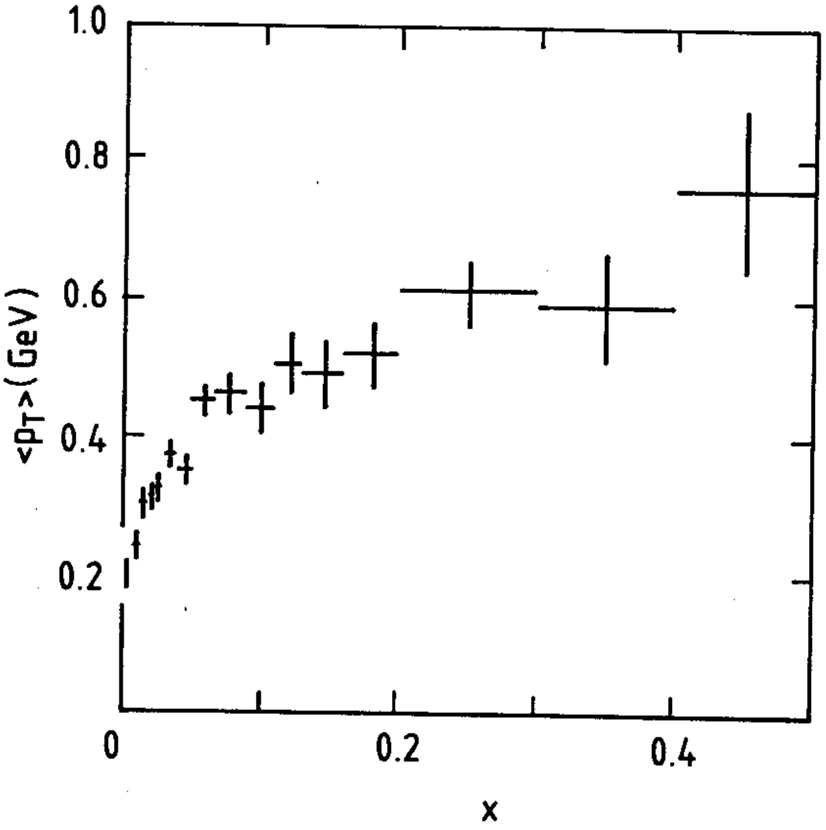

Fig. 14